

# Directly measuring single-molecule heterogeneity using force spectroscopy

Michael Hinczewski<sup>a,1</sup>, Changbong Hyeon<sup>b</sup>, and D. Thirumalai<sup>c</sup>

<sup>a</sup>Department of Physics, Case Western Reserve University, Cleveland, OH 44106; <sup>b</sup>Korea Institute for Advanced Study, Seoul 02455, Korea; and <sup>c</sup>Biophysics Program, Institute For Physical Science and Technology, University of Maryland, College Park, MD 20742

Edited by Ken A. Dill, Stony Brook University, Stony Brook, NY, and approved May 10, 2016 (received for review September 16, 2015)

**One of the most intriguing results of single-molecule experiments on proteins and nucleic acids is the discovery of functional heterogeneity: the observation that complex cellular machines exhibit multiple, biologically active conformations. The structural differences between these conformations may be subtle, but each distinct state can be remarkably long-lived, with interconversions between states occurring only at macroscopic timescales, fractions of a second or longer. Although we now have proof of functional heterogeneity in a handful of systems—enzymes, motors, adhesion complexes—identifying and measuring it remains a formidable challenge. Here, we show that evidence of this phenomenon is more widespread than previously known, encoded in data collected from some of the most well-established single-molecule techniques: atomic force microscopy or optical tweezer pulling experiments. We present a theoretical procedure for analyzing distributions of rupture/unfolding forces recorded at different pulling speeds. This results in a single parameter, quantifying the degree of heterogeneity, and also leads to bounds on the equilibration and conformational interconversion timescales. Surveying 10 published datasets, we find heterogeneity in 5 of them, all with interconversion rates slower than  $10\text{ s}^{-1}$ . Moreover, we identify two systems where additional data at realizable pulling velocities is likely to find a theoretically predicted, but so far unobserved crossover regime between heterogeneous and nonheterogeneous behavior. The significance of this regime is that it will allow far more precise estimates of the slow conformational switching times, one of the least understood aspects of functional heterogeneity.**

biomolecule heterogeneity | atomic force microscope | optical tweezers | rupture force distribution | dynamic disorder

One of the great problems in modern biology is to understand how the intrinsic diversity of cellular behaviors is shaped by factors outside of the genome. The causes of this heterogeneity are spread across multiple scales, from noise in biochemical reaction networks through epigenetic mechanisms like DNA methylation and histone modification (1). It might be natural to expect heterogeneity at the cellular level because of the bewildering array of time and length scales associated with the molecules of life that govern cell function. Surprisingly, even at the level of individual biomolecules, diversity in functional properties like rates of enzymatic catalysis (2–5) or receptor–ligand binding (6, 7) can occur. This diversity arises from the presence of many distinct functional states in the free-energy landscape, which correspond to long-lived active conformations of the biomolecule. Although the reigning paradigm in proteins and nucleic acids has been a single, folded native structure, well separated in free energy from any other conformations, possibilities about rugged landscapes with multiple native states have been explored for a long time (8–15). However, only with the revolutionary advances in single-molecule experimental techniques in recent years have we been able to gather direct evidence of functional heterogeneity, in systems ranging from protein enzymes (2–4) and nucleic acids (5, 16, 17), to molecular motors (18) and cell adhesion complexes (6, 7). As research inevitably moves toward larger macromolecular systems, the examples of functional heterogeneity will only multiply. We thus need to develop theories that can deduce aspects of the hidden kinetic network of states underlying

the single-molecule experimental data (19), allowing us to quantify the nature and extent of the heterogeneity.

The focus in this study is single-molecule force spectroscopy, conducted either by atomic force microscopy (AFM) or optical tweezers, which constitutes an extensive experimental literature over the last two decades. Our contention is that evidence of heterogeneity is widespread in this literature, but has gone largely unnoticed, because researchers [with a few exceptions, as discussed below (20–23)] did not recognize the markers in their data that indicated heterogeneous behavior. To remedy this situation, we introduce a universal approach to analyzing distributions of rupture/unfolding forces collected in pulling experiments, which yields a single nondimensional parameter  $\Delta \geq 0$ . The magnitude of  $\Delta$  characterizes the extent of the disorder in the underlying ensemble, the ruggedness of the free-energy landscape. Moreover, our method provides a way of estimating bounds on key timescales, describing both the fast local equilibration in each well (distinct system state) of our rugged landscape, and the slow interconversion between the various wells. After verifying the validity of our approach using synthetic data generated from a heterogeneous model system, we survey 10 experimental datasets, comprising a diverse set of biomolecular systems from simple DNA oligomers to large complexes of proteins and nucleic acids. The largest values of  $\Delta$  in our survey, indicating the strongest heterogeneity, come from systems involving nucleic acids alone or protein/nucleic acid interactions, supporting the hypothesis that nucleic acid free-energy landscapes are generally more rugged than those involving only proteins (24). Our theory thus provides a powerful new analytical tool, for the first time (to our knowledge) allowing a broad comparison of functional heterogeneity among different biomolecules through a common experimental protocol.

## Significance

The relationship between structure and function is the heart of modern cell biology. Technological innovations in manipulating single molecules of proteins, DNA/RNA, and their complexes, are beginning to reveal the surprising intricacies of this relationship. In certain cases, the same molecule randomly switches between various long-lived structures, each with different functional properties. We present a theory to extract the extent and dynamics of these structural fluctuations from single-molecule experimental data. We find large heterogeneity in DNA and RNA complexes, supporting the notion that energy landscapes involving nucleic acids are rugged. Our work shows that functional heterogeneity is far more common than previously thought and suggests experimental approaches for estimating the timescales of these fluctuations with unprecedented accuracy.

Author contributions: M.H., C.H., and D.T. designed research, performed research, analyzed data, and wrote the paper.

The authors declare no conflict of interest.

This article is a PNAS Direct Submission.

<sup>1</sup>To whom correspondence should be addressed. Email: mxh605@case.edu.

This article contains supporting information online at [www.pnas.org/lookup/suppl/doi:10.1073/pnas.1518389113/-DCSupplemental](http://www.pnas.org/lookup/suppl/doi:10.1073/pnas.1518389113/-DCSupplemental).

## Theory

**Force Spectroscopy for a Pure, Adiabatic System.** As a starting point, consider a generic free-energy landscape for a biomolecular system with a single functional state (Fig. 1A) subject to an increasing time-dependent external force  $f(t)$ . For a molecular complex, the functional basin of attraction in the landscape would correspond to an ensemble of bound conformations with similar energies, which we label N. For the case of single-molecule folding, this would be the unique native ensemble. The force is applied through an experimental apparatus like an AFM or optical tweezer, typically connected to the biomolecule through protein or nucleic acid linkers of known stiffness. The apparatus is pulled at a constant velocity  $v$ , leading to a force ramp with slope  $df/dt = \omega_s(f)v$ , where  $\omega_s(f)$  is the effective stiffness of the setup (linkers plus the AFM cantilever or optical trap). This  $\omega_s(f)$  may in general depend on the force, particularly for the AFM setup, where the cantilever

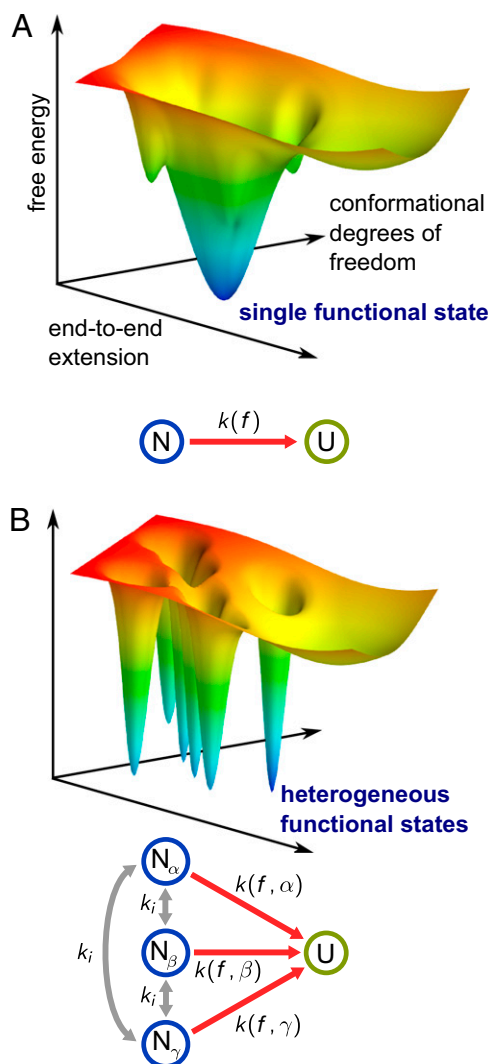


**Fig. 1.** (A) Schematic biomolecular free-energy landscape with a single functional state, N, corresponding to an ensemble of folded/bound conformations. Under an adiabatically increasing external force  $f(t)$ , there is an instantaneous rupture rate  $k(f(t))$  describing transitions between N and the unfolded/unbound ensemble U. (B) Schematic free-energy landscape of a heterogeneous system with multiple functional states. Each functional ensemble  $N_\alpha$  will have a state-dependent adiabatic rupture rate  $k(f, \alpha)$ . Assuming the states are roughly equally probable in equilibrium, there will be a single overall rate  $k_i$  for interconversion between the various states.

stiffness is often comparable to or greater than that of the molecular construct. So we also define a characteristic stiffness  $\bar{\omega}_s$ , which we set to the mean  $\omega_s(f)$  over the range of forces probed in the experiment (although the precise value of  $\bar{\omega}_s$  is not important). This allows us to introduce a characteristic force loading rate  $r$  proportional to the velocity,  $r = \bar{\omega}_s v$ .

If at time  $t=0$  the system starts in N, the force ramp tilts the landscape along the extension coordinate. If we model the conformational dynamics of the system as diffusion within this landscape, the tilting eventually leads to a transition out of N, associated with unbinding of the complex or unfolding of the molecule (an ensemble of states we call U). We let  $\Sigma_r(t)$  be the survival probability for loading rate  $r$ , in other words, the probability that the transition to U has not occurred by time  $t$ . The distribution of first rupture times is then  $-d\Sigma_r/dt$ , and the mean rupture rate  $\bar{k}(r)$  is just the inverse of the average rupture time:

$$\bar{k}(r) = \left[ \int_0^\infty dt t \left( -\frac{d\Sigma_r}{dt} \right) \right]^{-1} = \left[ \int_0^\infty dt \Sigma_r(t) \right]^{-1}, \quad [1]$$

where we have used integration by parts and assumed that rupture always occurs if we wait long enough,  $\Sigma_r(\infty) = 0$ .

The behavior of  $\Sigma_r(t)$  at different  $r$  depends on how  $\bar{k}(r)$  compares to two other intrinsic rates. The first is the equilibration rate  $k_{\text{eq}}$  in the N well, or how quickly the system samples the configurations of the functional ensemble. For a single, smooth well with mean curvature  $\omega_0$  and a diffusion constant  $D$ , this rate is on the order of  $k_{\text{eq}} \sim \beta \omega_0 D$ , where  $\beta = 1/k_B T$ . The second is a critical rate  $k_c(r) = r/f_c$ , which describes how quickly the force reaches a critical force scale for rupture  $f_c \sim G^\ddagger/x^\ddagger$ . Here,  $G^\ddagger$  is the energy scale of the barrier that needs to be overcome for the N-to-U transition at zero force, and  $x^\ddagger$  is the extension difference between the N well minimum and the transition state. For  $f \gtrsim f_c$ , the landscape is tilted sufficiently that the barrier becomes insignificant, and rupture occurs quickly (on a diffusion-limited timescale). If  $k_c(r) \ll \bar{k}(r) \ll k_{\text{eq}}$ , the system is in the adiabatic regime. The force ramp is sufficiently slow that rupture occurs before the critical force is reached, and equilibration is fast enough that the system can reach quasiequilibrium at the instantaneous value of the force  $f(t)$  at all times  $t$  before the rupture.

If the adiabatic condition is satisfied, the survival probability  $\Sigma_r(t)$  obeys the kinetic equation  $d\Sigma_r(t)/dt = -k(f(t))\Sigma_r(t)$ , where  $k(f)$  is the rupture rate at constant force  $f$ . Because  $f(t)$  is a monotonically increasing function of  $t$ , we can change variables from  $t$  to  $f(t)$  (25), and solve for  $\Sigma_r(f)$ , the probability that the system does not rupture before the force value  $f$  is reached:

$$\Sigma_r(f) = \exp\left(-\frac{1}{r} \int_0^f df' \frac{\bar{\omega}_s k(f')}{\omega_s(f')}\right). \quad [2]$$

Interestingly, the integral inside the exponential is independent of the loading rate  $r$ . Hence, for a system pulled from a single native ensemble, we can calculate the following quantity from experimental trajectories at different  $r$ :

$$\Omega_r(f) \equiv -r \log \Sigma_r(f), \quad [3]$$

and the results should collapse onto a single master curve for all  $r$  in the adiabatic regime. When  $r$  is sufficiently large that  $\bar{k}(r) < k_c(r)$  or  $\bar{k}(r) > k_{\text{eq}}$ , the assumption of quasiequilibrium on a slowly changing energy landscape breaks down, and Eq. 2 no longer holds. For this fast, nonadiabatic case (26, 27), we should find that  $\Omega_r(f)$  varies with  $r$ , as we will explore later in more detail.

**Force Spectroscopy for a Heterogeneous, Adiabatic System.** In a pioneering series of studies, Raible and collaborators (20–22) analyzed force ramp experiments for the regulatory protein ExpG unbinding

from a DNA fragment. Plotting  $\Omega_r(f)$  (the data reproduced in Fig. 6D), they did not find any collapse, as might be surmised from Eq. 3. This was not an artifact due to nonadiabaticity [violation of the inequality  $k_c(r) \ll \bar{k}(r) \ll k_{\text{eq}}$ ], because the absence of collapse becomes even more pronounced at small loading rates, further into the adiabatic territory where collapse should be observed. They correctly inferred that the cause of this divergence is heterogeneity in the ensemble of states in the protein–DNA complex.

To understand the behavior of  $\Omega_r(f)$  in a heterogeneous system, let us consider the effects of a force ramp on a biomolecular free-energy landscape with multiple functional states (Fig. 1B). Our goal is to use  $\Omega_r(f)$ , derived from experimental pulling trajectories, to quantify the extent of the heterogeneity and extract information about the underlying conformational dynamics. The functional states are distinct basins of attraction in the landscape, corresponding to distinct functional ensembles which we label  $N_\alpha$  for state  $\alpha$ . We assume the minimum energy in each well and their overall dimensions are comparable, so that the equilibrium probabilities  $p_\alpha^{\text{eq}}$  of the various states are of the same order. In this case, if  $\alpha \neq \alpha'$ , the transition rates  $k_{\alpha \rightarrow \alpha'}$  and  $k_{\alpha' \rightarrow \alpha}$  are also similar from detailed balance,  $k_{\alpha \rightarrow \alpha'}/k_{\alpha' \rightarrow \alpha} = p_\alpha^{\text{eq}}/p_{\alpha'}^{\text{eq}} \sim O(1)$ . Hence, we can introduce an overall scale for the interconversion rate between the different states,  $k_i$ , such that  $k_{\alpha \rightarrow \alpha'} \sim O(k_i)$  for any  $\alpha \neq \alpha'$ . Thus, we now have two intrinsic timescales:  $k_{\text{eq}}$  for equilibration within a single  $N_\alpha$ , and  $k_i$  for transitions between distinct  $N_\alpha$  values, where typically  $k_i \ll k_{\text{eq}}$  must be true in order to observe clear heterogeneity.

The experimental setup is the same as above, with a loading rate  $r$ , and a corresponding mean rupture rate  $\bar{k}(r)$  for reaching the U ensemble. We can identify three dynamical regimes, based on the magnitude of  $k_i$ . In the first regime, interconversion is slow, with  $k_i \ll \bar{k}(r)$ . In the second regime,  $k_i$  is comparable to  $\bar{k}(r)$ . In fact, as we will discuss later in more detail, we will be particularly interested in the crossover scenario where  $k_i \geq \bar{k}(r)$  for some subset of the  $r$  values in the experiment, but  $k_i < \bar{k}(r)$  for the remainder. If this second regime is identified in an experiment, it provides a way to estimate the scale of  $k_i$ . Finally, in the third regime, the barriers between the  $N_\alpha$  basins of attraction are small, such that  $k_i \gg \bar{k}(r)$ , and the system can sample all of the states before rupture. Qualitatively, this scenario is indistinguishable from the case of a system with a single native basin of attraction, with  $k_i$  taking the role of  $k_{\text{eq}}$  as the rate scale for overall equilibration in the landscape. Because the first regime is simpler to treat mathematically than the second regime, we will initially focus on a theory to describe the first regime and identify its signatures in experimental data. Assessing the validity of this theory in experiments will turn out to be a useful criterion for distinguishing between the first, second, and third regimes, and thus putting bounds on  $k_i$ . This by-product of our theory is of considerable importance because it is a priori very difficult to estimate  $k_i$ .

To begin, consider adiabatic pulling where  $k_i$  is the slowest rate in the system,  $k_i \ll k_c(r) \ll \bar{k}(r) \ll k_{\text{eq}}$ . On the timescale of pulling and rupture, the system is effectively trapped in a heterogeneous array of states: if we start a pulling trajectory in state  $\alpha$ , the system will remain in that state until rupture. The rupture rate at constant force,  $k(f, \alpha)$  will in general depend on the state, and the ensemble of molecules from which we pull will be characterized by a set of initial state probabilities  $p_\alpha$ . If  $k_i$  is extremely small, such that the system cannot interconvert even on the macroscopic timescales of experimental preparation,  $p_\alpha$  may be different from  $p_\alpha^{\text{eq}}$ , because we are not guaranteed to draw from an equilibrium distribution across the entire landscape. This distinction is not important for the analysis below. In fact, our approach also works when  $k_i = 0$ , corresponding to the quenched disorder limit, as seen for example in an ensemble of molecules with covalent chemical differences.

The analog of Eq. 2 for the survival probability  $\Sigma_r(f)$  during adiabatic pulling in a heterogeneous system with small  $k_i$  is as follows:

$$\Sigma_r(f) = \left\langle \exp \left( -\frac{1}{r} \int_0^f df' \frac{\bar{\omega}_s k(f', \alpha)}{\omega_s(f')} \right) \right\rangle, \quad [4]$$

where the brackets denote an average over the initial ensemble of states,  $\langle O(\alpha) \rangle \equiv \sum_\alpha p_\alpha O(\alpha)$  for any quantity  $O(\alpha)$ . The associated  $\Omega_r(f)$  from Eq. 3 can be expressed through a cumulant expansion in terms of the integrand  $I(f, \alpha) \equiv \int_0^f df' \bar{\omega}_s k(f', \alpha) / \omega_s(f')$  as follows:

$$\Omega_r(f) = - \sum_{n=1}^{\infty} (-1)^n \frac{\kappa_n(f)}{n! r^{n-1}}, \quad [5]$$

$$\kappa_n(f) \equiv \frac{\partial^n}{\partial \lambda^n} \log \langle e^{\lambda I(f, \alpha)} \rangle_{\lambda=0}.$$

The first two cumulants are  $\kappa_1(f) = \langle I(f, \alpha) \rangle$  and  $\kappa_2(f) = \langle I^2(f, \alpha) \rangle - \langle I(f, \alpha) \rangle^2$ . In the absence of heterogeneity, all cumulants  $\kappa_n(f)$  with  $n > 1$  are exactly zero. For a small degree of heterogeneity, or equivalently for sufficiently fast loading rates  $r$ , the main contribution to the expansion is from the  $n=1$  and  $n=2$  terms. For the case of fast  $r$ , we assume that we are still within the adiabatic regime, where  $k_c(r) \ll \bar{k}(r)$ , which turns out to be valid even for the largest loading rates in the experimental studies discussed below. In this scenario, where the  $n > 2$  contributions are negligible,  $\Omega_r(f)$  can be approximated as follows:

$$\Omega_r(f) \approx \frac{r}{\Delta(f)} \log \left( 1 + \frac{\kappa_1(f) \Delta(f)}{r} \right), \quad [6]$$

where  $\Delta(f) \equiv \kappa_2(f) / \kappa_1^2(f) \geq 0$  is a dimensionless measure of the ensemble heterogeneity. For a pure system,  $\Delta(f) \rightarrow 0$ , giving  $\Omega_r(f) \rightarrow \kappa_1(f)$ , independent of  $r$ . Eq. 6 agrees with the expansion in Eq. 5 up to order  $n=2$ , and also has the nice property that it satisfies the inequality  $\Omega_r(f) \leq \kappa_1(f)$ , just like the exact form. The latter inequality follows from the definition of  $\Sigma_r(f)$  in Eq. 4 and Jensen's inequality,  $\Sigma_r(f) \geq \exp(-\kappa_1(f)/r)$ .

**Implementing the Model on Experimental Data.** So far, the discussion has been completely general, but to fit Eq. 6 to experimental data we need specific forms for  $\Delta(f)$  and  $\kappa_1(f)$ . The minimal physically sensible approximation, with the smallest number of unknown parameters, supplements Eq. 6 with the following assumptions:

$$\Delta(f) = \Delta, \quad \kappa_1(f) = \frac{k_0}{\beta x^\ddagger} \left( e^{\beta f x^\ddagger} - 1 \right). \quad [7]$$

The constants  $\Delta$ ,  $k_0$ , and  $x^\ddagger$  are fitting parameters. This presumes that  $\Delta(f)$  changes little over the range of forces in the data, and  $\kappa_1(f)$  has the same mathematical form as in a pure Bell model with an escape rate  $k(f) = k_0 e^{\beta f x^\ddagger}$  and  $\omega_s(f) = \bar{\omega}_s$ , where  $k_0$  is the escape rate at zero force and  $x^\ddagger$  is the distance to the transition state. For a heterogeneous system, the parameters  $k_0$  and  $x^\ddagger$  no longer have this simple interpretation, but we can still treat them as effective Bell values, averaged over the ensemble, with  $\Delta$  measuring the overall scale of the heterogeneity. Eq. 6, together with the three-parameter approximation of Eq. 7, provides remarkably accurate fits to all of the heterogeneous experimental datasets we have encountered in the literature. As will be seen below, it is capable of simultaneously fitting  $\Omega_r(f)$  data for loading rates  $r$  spanning nearly two orders of magnitude.

Although we focus on  $\Omega_r(f)$  as the main experimental quantity of interest, Eqs. 6 and 7 can also be used to derive a closed form expression for the probability distribution of rupture forces,  $p_r(f) = -d\Sigma_r(f)/df = -(d/df) \exp(-\Omega_r(f)/r)$ , at loading rate  $r$ :

$$p_r(f) = \frac{k_0 e^{\beta f x^\ddagger}}{r} \left( 1 + \frac{\Delta k_0 (e^{\beta f x^\ddagger} - 1)}{\beta r x^\ddagger} \right)^{-\frac{\Delta+1}{\Delta}}. \quad [8]$$

In the limit of no heterogeneity,  $\Delta \rightarrow 0$ , this distribution reduces to the one predicted for a Bell model under a constant loading

rate (25). The theoretical form for  $p_r(f)$  also allows us to carry out a relative likelihood analysis on the experimental data, to verify that  $\Delta$  is indeed a robust indicator of heterogeneity. As detailed in *Supporting Information, 6. Relative Likelihood Analysis of Heterogeneous vs. Pure Model Fitting for Experimental Data*, we found that experimental distributions  $p_r(f)$  corresponding to systems with nonzero  $\Delta$  were far more likely to be described by the heterogeneous theory in Eq. 8 than a pure model with the same number of parameters. We

surmise that if analysis of experimental data using our theory indicates that  $\Delta \neq 0$  then it is highly probable that a multiple state description is needed, thus dismissing a one-dimensional pure state description.

To verify that our analysis and conclusions would not change substantially even if the assumptions of the minimal model were relaxed, we have also tested two generalized versions of the model: one using the Dudko–Hummer–Szabo (28) instead of the Bell form for the escape rate in  $\kappa_1(f)$ , and the other allowing  $\Delta(f)$

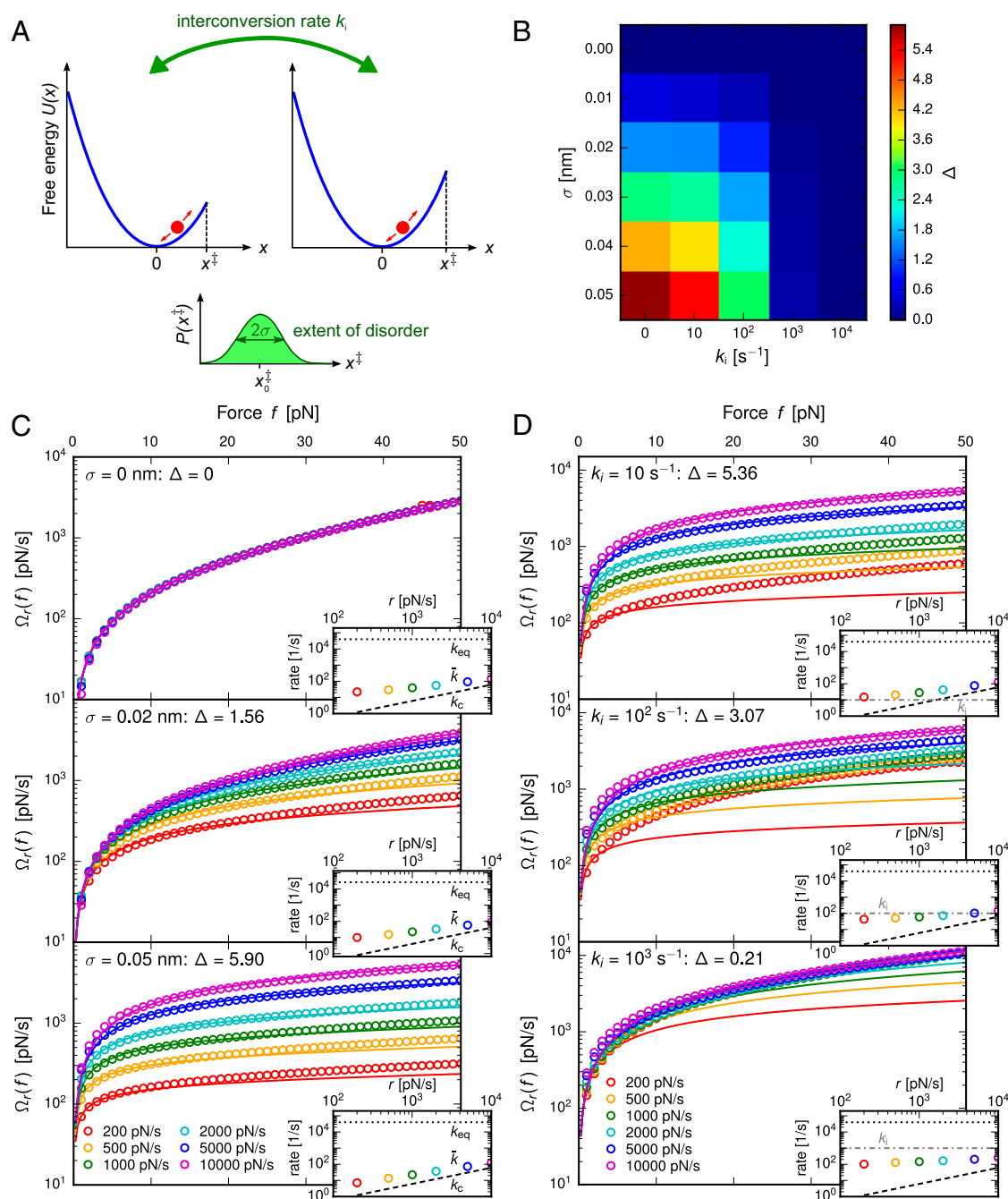


**Fig. 2.** Analysis of the FBL heterogeneous model system. (A) Two different free-energy wells, corresponding to distinct states, characterized by different transition distances to rupture,  $x^\ddagger$ . The system switches to a new value of  $x^\ddagger$ , drawn from a Gaussian distribution centered at  $x_0^\ddagger$  with SD  $\sigma$ , with rate  $k_i$ . (B) Heat map of  $\Delta$  as it varies with  $\sigma$  and  $k_i$ , extracted from fitting the theory of Eqs. 6 and 7 to numerical simulation results of  $\Omega_r(f)$  for the model system. The parameters are as follows:  $D = 100$  nm $^2$ /s,  $\omega_0 = 400$   $k_B T$ /nm $^2$ ,  $x_0^\ddagger = 0.2$  nm,  $\sigma = 0$ –0.05 nm, and  $k_i = 0$ – $10^4$  s $^{-1}$ . (C and D) Sample simulation results  $\Omega_r(f)$  (circles) on a logarithmic scale, with each color denoting a different loading rate  $r$ . The panels show different combinations of  $k_i$  and  $\sigma$ , with the plots in C illustrating the case of quenched disorder ( $k_i = 0$ ) for increasing  $\sigma$ , and  $D$  showing increasing  $k_i$  for fixed  $\sigma = 0.05$  nm. The theoretical best-fit curves are drawn as solid curves, and the resulting  $\Delta$  value is listed in each plot. The insets show the mean rupture rate  $\bar{k}(r)$  (circles) as a function of  $r$  compared with  $k_{eq}$  (dotted line),  $k_c(r)$  (dashed line), and  $k_i$  (dash-dotted line).

to vary linearly with  $f$  across the force range. Both extensions have four instead of three fitting parameters, but the heterogeneity results for the experimental systems we analyzed are completely consistent with those obtained using the minimal model (see [Supporting Information, 1. Testing the Assumptions of the  \$\Omega\_r\(f\)\$  Model with Respect to Possible Generalizations](#), for details). These results demonstrate that, if the need arises in future experimental contexts, the theory leading to Eq. 6 is quite general, and can be tailored by choosing suitable expressions for  $\kappa_1(f)$  and  $\Delta(f)$  that go beyond the minimal model of Eq. 7.

The theory described up to now applies only to the first dynamical regime, where  $k_i \ll \bar{k}(r)$ . However, the cases where  $k_i$  is larger than some or all of the  $\bar{k}(r)$ , and the theory partially or completely fails, turn out to be very informative as well. To understand these points, it is easier to discuss the theory in the context of a concrete physical model for heterogeneity, which we introduce in the next section.

## Results and Discussion

**Fluctuating Barrier Location Model.** Before turning to experimental data, we verify that the  $\Delta$  parameter extracted from the fitting of  $\Omega_r(f)$  curves using Eqs. 6 and 7 is a meaningful measure of heterogeneity. To do this, we will generate synthetic rupture data from a heterogeneous model system. The fluctuating barrier location (FBL) model, illustrated in Fig. 2A, consists of a reaction coordinate  $x$  whose dynamics are described by diffusion with constant  $D$  along a parabolic free energy  $U(x) = (1/2)\omega_0 x^2$  for  $x \leq x^\ddagger$ . Rupture occurs if  $x$  exceeds the transition distance  $x^\ddagger$ . To mimic dynamic heterogeneity, the value of  $x^\ddagger$  changes at random intervals, governed by a Poisson process with an interconversion rate  $k_i$ . At every switching event, a new value of  $x^\ddagger$  is drawn from a Gaussian probability distribution  $P(x^\ddagger) = \exp(-(x^\ddagger - x_0^\ddagger)^2 / 2\sigma^2) / \sqrt{2\pi\sigma^2}$  centered at  $x_0^\ddagger$  with SD  $\sigma$ , and diffusion continues if  $x$  is less than the transition distance. At time  $t = 0$ , when the applied force ramp  $f(t) = \tau t$  begins, we assume the initial ensemble of systems all start at  $x = 0$  with  $x^\ddagger$  values distributed according to  $P(x^\ddagger)$ . Survival probabilities  $\Sigma_r(f)$  are computed from numerical simulations of the diffusive process, with about  $3 \times 10^4$  rupture events collected for each parameter set (see [Supporting Information, 2. Heterogeneous Model Simulation Details](#), for additional details). The simplicity of the model, where one parameter,  $\sigma$ , controls the degree of heterogeneity, and another,  $k_i$ , the interconversion dynamics, allows us to explore the behavior of  $\Sigma_r(f)$ , and hence  $\Omega_r(f)$ , over a broad range of disorder and intrinsic timescales.

The circles in Fig. 2C and D show simulation results for  $\Omega_r(f)$  between  $f = 0$ –50 pN, plotted on a logarithmic scale, with each color denoting a different ramp rate in the range  $r = 200$ –10,000 pN/s. The model parameters are  $D = 100$  nm<sup>2</sup>/s,  $\omega_0 = 400$  k<sub>B</sub>T/nm<sup>2</sup>,  $x_0^\ddagger = 0.2$  nm,  $\sigma = 0$ –0.05 nm,  $k_i = 0$ –10<sup>4</sup> s<sup>−1</sup>, which give a variety of  $\Omega_r(f)$  curves of comparable magnitude over similar force scales to the experimental data discussed below. Fig. 2C shows results for quenched disorder ( $k_i = 0$ ) at different  $\sigma$ , whereas Fig. 2D shows results for varying  $k_i$  at fixed  $\sigma = 0.05$  nm. For a given choice of  $k_i$  and  $\sigma$ , we fit the analytical form of Eqs. 6 and 7 simultaneously to the six  $\Omega_r(f)$  curves at different  $r$ , with the best-fit model plotted as solid lines in Fig. 2C and D. This fitting yields values for  $\Delta$ ,  $k_0$ , and  $x^\ddagger$  in each case. The variation of  $\Delta$  with  $\sigma$  and  $k_i$  is plotted as a heat map in Fig. 2B.

Let us first consider the quenched disorder results (Fig. 2C and the left column of Fig. 2B). By definition, because  $k_i = 0$ , the system ensemble is permanently frozen in a heterogeneous array of different states with different values of  $x^\ddagger$ . Moreover, the adiabatic assumptions also hold, as can be seen in the *Insets* to Fig. 2C. These show the mean rupture rate  $\bar{k}(r)$  for different  $r$  (circles) compared with  $k_{\text{eq}}$  (dotted line) and  $k_c(r)$  (dashed line). For all of the  $r$  values analyzed,  $k_c(r) < \bar{k}(r) \ll k_{\text{eq}}$ , so adiabaticity should approximately hold. Thus, the assumptions leading to Eqs. 6 and 7 are valid, and indeed the analytical form provides an excellent fit to the simulation data. Although the theory is by construction most accurate in the

limit of fast (but still adiabatic)  $r$ , it still quantitatively describes the results for  $r$  spanning two orders of magnitude. Only small discrepancies start to appear at the slowest loading rates. For the pure system limit ( $\sigma = 0$ ), the best-fit value of  $\Delta$  is also zero, with all of the  $\Omega_r(f)$  curves collapsing on one another.  $\Delta$  progressively increases with  $\sigma$ , growing roughly proportional to the width of the disorder distribution. The greater the heterogeneity, the more pronounced the separation between the  $\Omega_r(f)$  curves at various  $r$ .

The results in Fig. 2D are obtained by keeping the extent of heterogeneity fixed at a large level ( $\sigma = 0.05$  nm) and allows interconversion, increasing  $k_i$  from 10 to 10<sup>3</sup> s<sup>−1</sup>. So long as  $\bar{k}(r) \gg k_i$ , the system is unlikely to interconvert on the timescale of rupture, and we see distinct, noncollapsed  $\Omega_r(f)$  curves. However, as  $k_i$  increases and overtakes  $\bar{k}(r)$ , starting from the smallest values of  $r$  where  $\bar{k}(r)$  has the smallest magnitude, the  $\Omega_r(f)$  curves begin to collapse on one another. This leads to increasing discrepancies between the data and the theoretical fit, because the assumptions justifying the theory break down when  $\bar{k}(r) < k_i$ . Eventually, once  $k_i$  is greater than all of the  $\bar{k}(r)$ , there is total collapse of the  $\Omega_r(f)$  curves (Fig. 2D, *Bottom*). Frequent interconversion between the different states of the system before rupture averages out the heterogeneity, making the results indistinguishable from a pure system. In this limit, the ensemble of functional states acts effectively like a single functional basin of attraction, with multiple distinct pathways to rupture. Although multiple pathways between a pair of states can be considered to be another manifestation of heterogeneity, they are not in themselves sufficient to lead to noncollapse of the  $\Omega_r(f)$  curves, as we discuss in more detail in [Supporting Information, 3. Heterogeneity in Rupture Pathways vs. Heterogeneity in Functional States](#). To see anything but complete collapse of the  $\Omega_r(f)$  curves in the adiabatic regime requires a small enough interconversion rate  $k_i$ , slower than the mean rupture rates  $\bar{k}(r)$  for at least some subset of the  $r$  values.

## Dynamical Regimes and Extraction of Bounds on Timescales of Internal Dynamics.

Interestingly, it is precisely the discrepancy in the theoretical fits with increasing  $k_i$  that points the way to one of the most valuable features of our approach. Not only can we measure heterogeneity, but we can also infer information about the timescales of conformational dynamics. Note first that the best-fit values of  $\Delta$  track the disappearance of heterogeneity, monotonically decreasing from  $\Delta = 5.90$  at  $\sigma = 0.05$ ,  $k_i = 0$  s<sup>−1</sup>, to  $\Delta = 0.21$  at  $\sigma = 0.05$ ,  $k_i = 10^3$  s<sup>−1</sup>. It is clear, however, that as  $k_i$  increases and dynamical disorder becomes more prominent, a single overall value of  $\Delta$  is an imperfect description of the dynamics. Instead of obtaining a single  $\Delta$  value by simultaneously fitting all the  $\Omega_r(f)$  curves at multiple  $r$ , we can get a more fine-grained picture by looking at  $\Delta$  calculated from smaller subsets of the data, and how it varies with the mean timescale of rupture  $\bar{k}$ . To accomplish this, let us take  $\Omega_r(f)$  curves from two consecutive loading rates ( $r_1, r_2$ ), fit Eqs. 6 and 7, and calculate the resulting value of  $\Delta$ , which we will call the “pair” parameter  $\Delta_p(r_1, r_2)$ . For example, if our total dataset consists of six loading rates  $r = 200, 500, 1,000, 2,000, 5,000, 10,000$  pN/s, we first determine  $\Delta_p(r_1, r_2)$  for  $(r_1, r_2) = (200, 500)$  pN/s, then  $(500, 1,000)$  pN/s, and so on, to get five different results for  $\Delta_p(r_1, r_2)$ . The advantage of this approach is that each  $\Delta_p$  corresponds to a much smaller range of rupture timescales than what is covered by the entire dataset. In Fig. 3A, we plot  $\Delta_p$  for  $\sigma = 0.05$ ,  $k_i = 0, 10, 10^2, 10^3$  s<sup>−1</sup>. The  $x$ -axis coordinate is the smaller mean rupture rate of the pair,  $\bar{k} = \min(\bar{k}(r_1), \bar{k}(r_2))$ .

The results for  $\Delta_p$  in Fig. 3A allow us to identify three different behaviors, corresponding to the three dynamical regimes discussed in *Theory*:

- i) Noncollapse (NC): Here, all of the  $\Delta_p(r_1, r_2) \geq 1$ , and  $\Delta_p(r_1, r_2)$  for any pair of  $(r_1, r_2)$  is approximately the same as  $\Delta$  calculated from the entire dataset. We see this in the

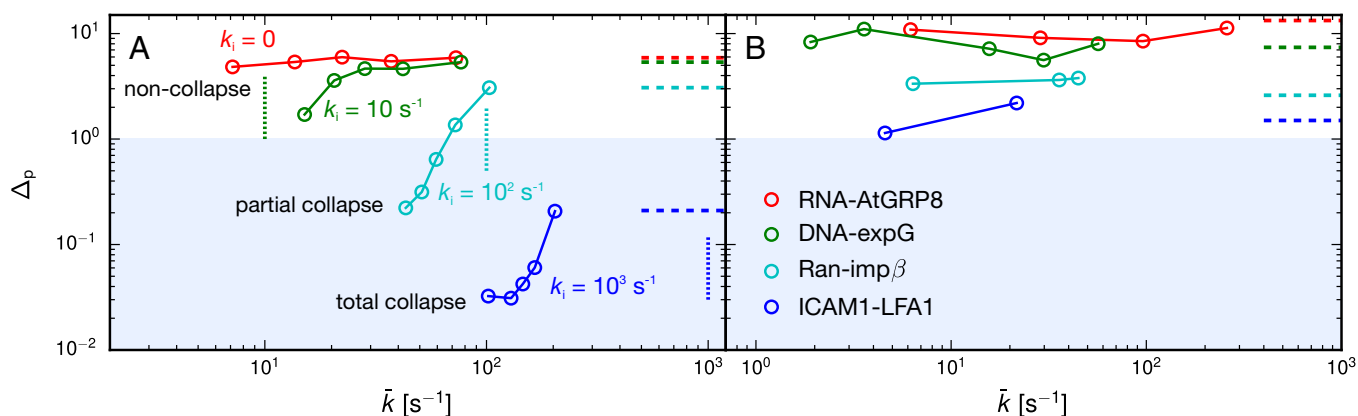


**Fig. 3.** Pair heterogeneity parameter  $\Delta_p$ , calculated from a best fit of  $\Omega_r(f)$  curves for two consecutive values of loading rate ( $r_1, r_2$ ) in a given dataset. The horizontal axis coordinate is the smaller of the mean rupture rates for each pair,  $\bar{k} = \min(\bar{k}(r_1), \bar{k}(r_2))$ . For comparison, the  $\Delta$  calculated from all loading rates in a dataset is shown as a horizontal dashed line. The shaded region corresponds to  $\Delta_p \leq 1$ , where disorder is negligible. (A) Results for the FBL model system of Fig. 2, with  $\sigma = 0.05$  nm and  $k_i = 0, 10, 10^2$ , and  $10^3$  s $^{-1}$ . From *Left to Right*, the  $\Delta_p$  points for each  $k_i$  value correspond to loading rate pairs:  $(r_1, r_2) = (200, 500), (500, 1,000), (1,000, 2,000), (2,000, 5,000),$  and  $(5,000, 10,000)$  pN/s. Vertical dotted lines mark the values of  $k_i$  in each case. Systems where  $\Delta_p \geq 1$  across all measured timescales of  $\bar{k}(r)$  must have slow conformational interconversion,  $k_i < \bar{k}(r)$  or static disorder ( $k_i = 0$ ), and thus correspond to the noncollapse (NC) regime. When some  $\bar{k}(r)$  are larger than  $k_i$  and some are smaller, we are in the partial collapse (PC) regime, with smaller  $\bar{k}(r)$  exhibiting  $\Delta_p \ll 1$ , and the larger ones  $\Delta_p \geq 1$ . When  $k_i > \bar{k}(r)$  for the entire dataset, all  $\Delta_p \ll 1$ , and we are in the total collapse (TC) regime. (B) Results for four experimental systems (Fig. 6) that exhibit heterogeneity and have datasets with at least three loading rates. The  $\Delta_p$  calculated from pairs of loading rates are consistent with the  $\Delta$  calculated from the total dataset, and all fall in the  $\Delta_p \geq 1$  NC regime.

$k_i = 0$  s $^{-1}$  case in Fig. 3A, where for comparison the value of  $\Delta$  over the whole set is marked by a horizontal dashed line. The corresponding  $\Omega_r(f)$  curves are in Fig. 2C, Bottom. The agreement between  $\Delta_p(r_1, r_2)$  and  $\Delta$  is a consistency check for the theory, and implies that the underlying assumptions are valid, namely  $k_i < \bar{k}(r) < k_{eq}$  for all  $r$  in the dataset. From this, we can conclude that the minimum value of  $\bar{k}(r)$  among all of the loading rates  $r$  used in the experiment gives us an upper bound on  $k_i$ . Similarly the maximum value of  $\bar{k}(r)$  over all  $r$  gives a lower bound on  $k_{eq}$ . For  $k_i = 10$  s $^{-1}$  in Fig. 3A, we see what happens as  $k_i$  approaches the timescale of  $\bar{k}(r)$ . We are still in the NC regime, because  $\Delta_p \geq 1$  and  $k_i$  (vertical dotted line) is smaller than any of the  $\bar{k}(r)$ . However,  $k_i$  is now sufficiently close to  $\bar{k}(r = 200$  pN/s) that  $\Delta_p(200, 500)$  (the leftmost point) is smaller than the rest of the  $\Delta_p$ , which lie at faster rupture timescales relatively unaffected by  $k_i$ .

- ii) Partial collapse (PC):  $\Delta_p(r_1, r_2) \geq 1$  for the largest values of  $(r_1, r_2)$ , but for small loading rates  $\Delta_p(r_1, r_2) \ll 1$ . This occurs in the  $k_i = 10^2$  s $^{-1}$  results in Fig. 3A. In this regime, the system is adiabatic,  $k_{eq} > \bar{k}(r)$ , but now  $k_i$  falls between the smallest and largest values of  $\bar{k}(r)$ . In the  $k_i = 10^2$  s $^{-1}$  case, the variation in  $\Delta_p$  is a reflection of the degree of overlap in the  $\Omega_r(f)$  curves (Fig. 2D, Middle). The  $(r_1, r_2) = (5,000, 10,000)$  pN/s pair (blue and purple  $\Omega_r(f)$  circles) are clearly separated, corresponding to  $\Delta_p \geq 1$  and the fact that  $k_i \lesssim \bar{k}(r_1), \bar{k}(r_2)$ . The  $(200, 500)$  pN/s pair (red and orange circles) are nearly overlapping, corresponding to  $\Delta_p \ll 1$ , and  $k_i > \bar{k}(r_1), \bar{k}(r_2)$ . The PC regime thus provides the best case scenario for directly estimating  $k_i$  from the data, because we can bound  $k_i$  from above and below, and we know  $k_i$  will roughly coincide with the  $\bar{k}$  where  $\Delta_p(r_1, r_2) \sim 1$ .
- iii) Total collapse (TC):  $\Delta_p(r_1, r_2) \ll 1$  for all  $(r_1, r_2)$  in the dataset. This is illustrated by the  $k_i = 1,000$  s $^{-1}$  case in Fig. 3A, corresponding to the  $\Omega_r(f)$  curves in Fig. 2D, Bottom.  $\Delta_p$  values close to zero translate into near total overlap of the  $\Omega_r(f)$  results. This regime requires adiabaticity,  $k_{eq} > \bar{k}(r)$ , and if there is any heterogeneity in the system, the interconversion between states has to be fast,  $k_i > \bar{k}(r)$ . Thus, the maximum value of  $\bar{k}(r)$  over all  $r$  gives a lower bound on both  $k_i$  and  $k_{eq}$ .

To summarize, we can use the magnitude of the heterogeneity parameters ( $\Delta$  or  $\Delta_p$  depending on whether we look at the whole

dataset or pairs of ramp rates) to make specific inferences about the nature of the biomolecular free-energy landscape.  $\Delta \gg 1$  (large disorder) in an experimental dataset implies the following facts: there is an ensemble of folded/intact states in the system, these states have substantially different force-dependent rates of rupture, and the system will only rarely switch from one state to another before rupture occurs. A small but finite  $\Delta$  in the range  $0 \ll \Delta \lesssim 1$  (low disorder) indicates that heterogeneity is still present, but one or both of the following are true: the interconversion rate  $k_i$  is comparable to the mean rupture rates, so heterogeneity is partially averaged out due to transitions between states, or the differences in rupture rate functions between states are small. Finding  $\Delta \approx 0$  (no disorder) indicates that either there is no heterogeneity (a single native state) or that  $k_i$  is so large that the ensemble of native states behaves effectively like a single state.

**Ruling Out Nonadiabatic Artifacts.** One important question about the usefulness of the theory remains: what about situations where the loading rate  $r$  is sufficiently fast that the adiabatic assumption  $k_c(r) \ll \bar{k}(r) \ll k_{eq}$  breaks down? As mentioned above,  $\Omega_r(f)$  in this case will not collapse onto a single master curve independent of  $r$ , regardless of the presence of underlying heterogeneity in the system. Because the experimentalist has no direct way of measuring  $k_{eq}$  or  $k_c(r)$ , it is not a priori clear whether a given loading rate  $r$  is slow enough for adiabaticity to hold. Can the theory in Eqs. 6 and 7 fit a pure system over a range of nonadiabatic  $r$ , and yield a nonzero fitted value of  $\Delta$  that would incorrectly indicate the presence of heterogeneity? To rule out the possibility of such a false positive, we simulated the FBL model system above, without any heterogeneity ( $\sigma = 0$ ), over a much larger range of loading rates  $r$ , and plotted the results of  $\Omega_r(f)$  in Fig. 4 on a logarithmic scale for  $r = 10^3$  to  $5 \cdot 10^7$  pN/s. As shown in the figure *Inset*, for  $r \lesssim 10^5$  pN/s,  $\bar{k}(r)$  still falls between  $k_c(r)$  and  $k_{eq}$ , so adiabaticity holds and the  $\Omega_r(f)$  curves are nearly indistinguishable. However, for  $r \gtrsim 10^5$  pN/s, the collapse begins to break down, and the  $\Omega_r(f)$  curves grow increasingly distinct. Crucially, this nonadiabatic trend for a pure system is qualitatively different from what happens in the adiabatic heterogeneous case. In the former, the curves on a logarithmic plot grow more and more separated as  $r$  grows (Fig. 4), whereas in the



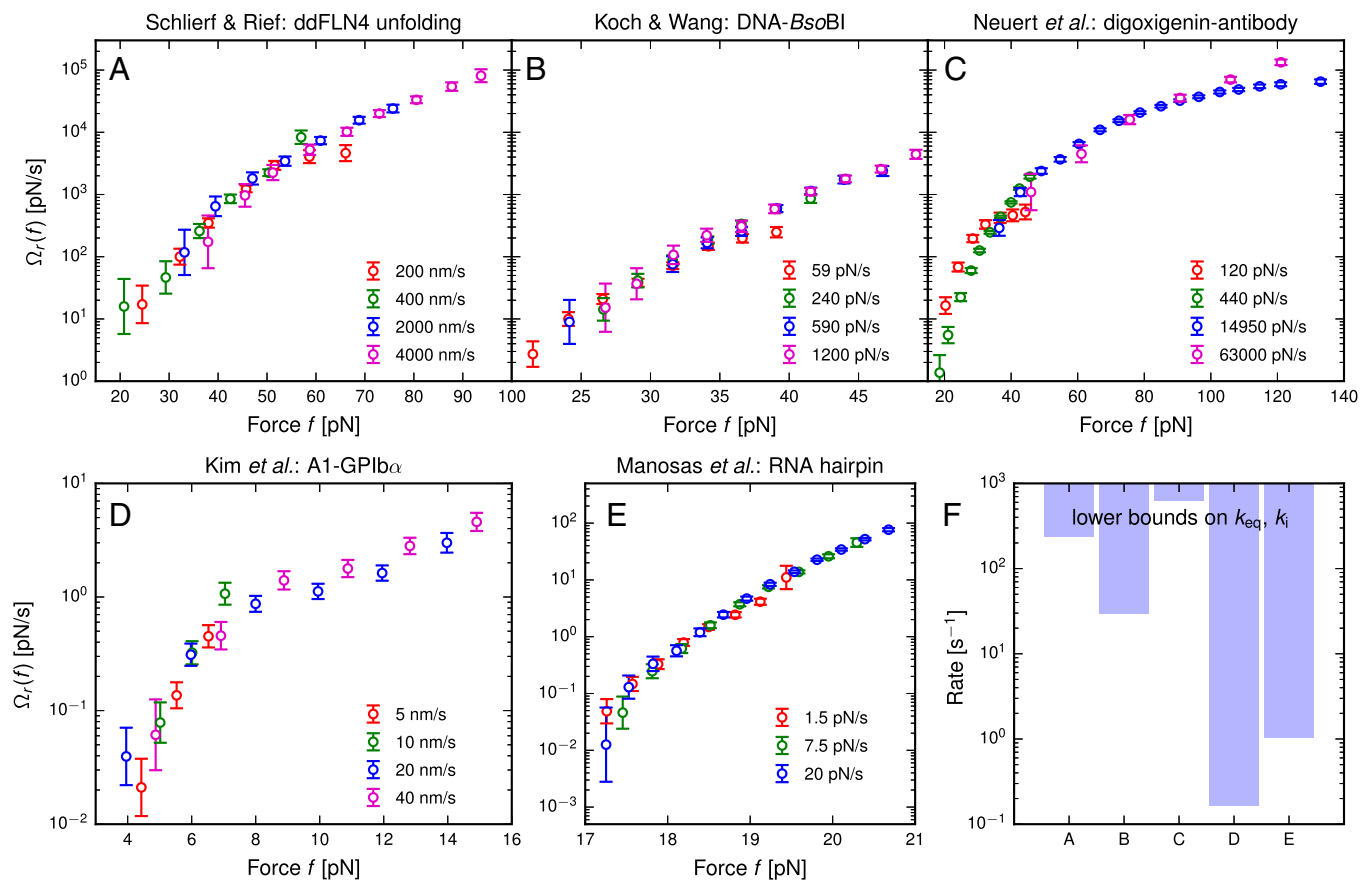


**Fig. 5.** Experimental  $\Omega_r(f)$  data (circles) calculated from rupture force distributions in five studies: (A) ref. 29, (B) ref. 30, (C) ref. 31, (D) ref. 6, and (E) ref. 32. All these cases exhibit no apparent heterogeneity, with the  $\Omega_r(f)$  curves for each system collapsing on one another. Colors denote different pulling velocities  $v$  or loading rates  $r$ , as reported in each study. For A and D, where  $v$  is reported, the linker stiffness values of  $\bar{w}_s = 4.1$  (A) and  $0.043$  pN/nm (D) are used to get the corresponding loading rates  $r = \bar{w}_s v$ . (F) For each of the experimental cases, the lower bounds on the possible values of  $k_{eq}$  and  $k_i$ , derived from the theoretical analysis.

(LFA1) integrin from its ligand, intercellular adhesion molecule-1 (ICAM1) (34); (B) rupture of the GTPase protein Ran from the nuclear receptor importin  $\beta$  (imp $\beta$ ) (35); for this dataset, Ran is loaded with a GTP analog (GppNHp), as well complexed with another binding partner, the protein RanBP1; (C) unzipping of a 10-bp DNA duplex (36); (D) Raible et al. (22) (based on earlier experimental data from ref. 37), the unbinding of the regulatory protein expG from a promoter DNA fragment; (E) Fuhrmann et al. (38), the unbinding of the protein ATGRP8 (in the mutant ATGRP8-RQ form) from its RNA target.

In all of these cases, the theoretical fit to Eqs. 6 and 7 (solid curves) is excellent, allowing us to extract the fitting parameters listed in each panel of Fig. 6. The values of  $k_0$ , the effective zero-force off-rate, are in the range  $\sim \mathcal{O}(0.01 - 0.1)$  s, whereas the effective transition state distance  $b \sim \mathcal{O}(0.1 - 1)$  nm. Both of these scales are physically sensible for protein or nucleic acid systems. The panels in Fig. 6 are ordered by increasing  $\Delta$ , which varies from 1.5 to 13.3. To verify the robustness of these  $\Delta$  values, we also calculated the pair parameters  $\Delta_p$  for every dataset that had at least three different loading rates. These are shown in Fig. 3B, with the corresponding  $\Delta$  for the full data indicated as horizontal dashed lines. As is expected for the NC regime, the  $\Delta_p$  do not vary significantly with rupture rate, and are consistent with  $\Delta$  in each case. The three largest values of  $\Delta$  (Fig. 6 C–E) correspond to bonds composed of nucleic acid base pairing or protein/nucleic acid interactions. This significant heterogeneity may reflect the tendency for free-energy landscapes involving nucleic acids to be more intrinsically rugged. However, it is not necessarily the case that all nucleic acid systems

are heterogeneous (the BsoBI–DNA complex of Fig. 5B and the RNA hairpin of Fig. 5E are counterexamples).

All of the data in Fig. 6 were collected using AFM pulling experiments, in contrast to Fig. 5, where B, D, and E were optical-trap results (the rest being AFM). It is thus worthwhile to wonder whether aspects of the AFM experimental setup could affect the heterogeneity analysis. In *Supporting Information, 5. Sensitivity of the Heterogeneity Analysis to Experimental Artifacts*, we have analyzed possible errors from several sources: the finite force resolution of AFM cantilever, the nonnegligible hydrodynamic drag on the cantilever at large pulling speeds ( $>1$   $\mu\text{m/s}$ ) (39–41), uncertainties arising from finite sampling of the rupture force distributions, and the apparatus response time. Based on this error analysis, we conclude that the estimation of the heterogeneity parameter  $\Delta$  from the experimental data are reliable in all of the systems of Fig. 6. The observed heterogeneity must therefore be an intrinsic aspect to the biomolecules, rather than an artifact of the AFM experiment.

The fidelity of the theoretical fits to the data in Fig. 6 (with no signs of PC) means all of the experiments were in the heterogeneous, adiabatic regime. Thus, the range of observed  $\bar{k}(r)$  allows us to place upper bounds on  $k_i$  and lower bounds on  $k_{eq}$ , which are plotted in the bar chart of Fig. 6F. There is a clear separation of timescales, with all of the upper bounds on  $k_i \lesssim 10$  s $^{-1}$ , and the lower bounds on  $k_{eq} \gtrsim 10^2$  s $^{-1}$ . The slow interconversion rates  $k_i$  in these systems are remarkable, particularly the DNA oligomer in Fig. 6C, which is a tiny system only 10 bp long. The rupture force distributions for the DNA unzipping were earlier fit to a specific model of dynamic disorder in ref. 23, where force-dependent rates of conformational



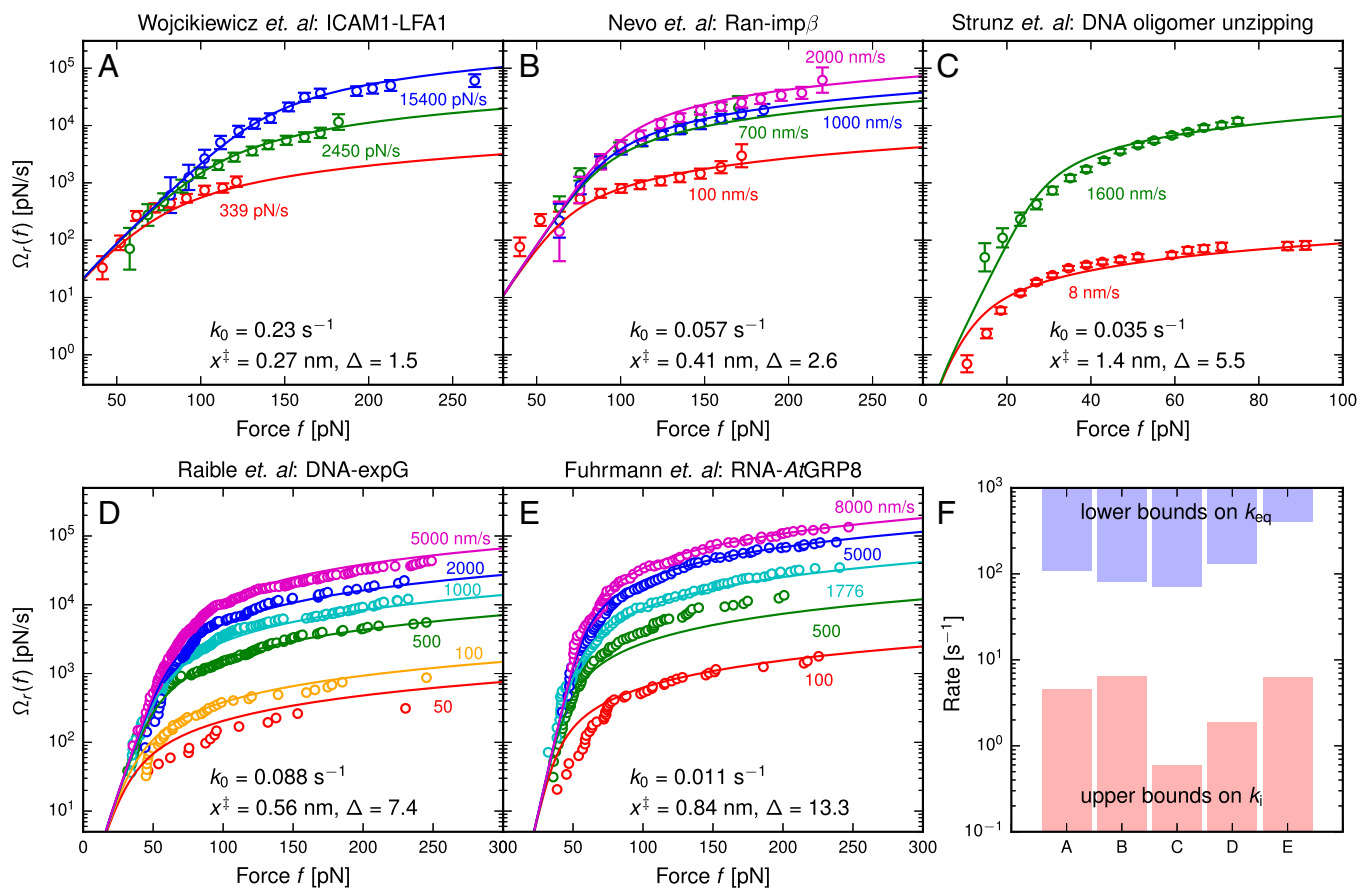


**Fig. 6.** Experimental  $\Omega_r(f)$  data (circles) calculated from rupture force distributions in five studies: (A) ref. (34), (B) ref. (35), (C) ref. (36), (D) ref. (22), and (E) ref. (38). In contrast to Fig. 5, these systems exhibit heterogeneity, with distinct  $\Omega_r(f)$  curves. Colors denote different pulling velocities  $v$  or loading rates  $r$ , as reported in each study. For B–E, where  $v$  is reported, the linker stiffness values of  $\bar{w}_s = 5.0$  (B), 2.0 (C), 3.0 (D), and 6.0 pN/nm (E) are used to get the corresponding loading rates  $r = \bar{w}_s v$ . Solid curves show the theoretical best fit to Eqs. 6 and 7, with the fitted parameters  $k_0$ ,  $x^\ddagger$ , and  $\Delta$  listed in each panel. (F) For each of the experimental cases, the lower bounds on the possible values of  $k_{\text{eq}}$  (blue bars) and the upper bounds on  $k_i$  (pink bars), derived from the theoretical analysis.

fluctuations were extracted. The range of these estimated rates ( $2.8 \times 10^{-5}$  to  $4.8 \times 10^{-1} \text{ s}^{-1}$ ) are consistent with the upper bound derived from the current analysis,  $k_i < 0.6 \text{ s}^{-1}$ . However, we must keep in mind that—unless PC is observed, pinpointing the scale of  $k_i$ —our analysis cannot distinguish between a heterogeneous system characterized by dynamic disorder with slow  $k_i$  and one with quenched disorder ( $k_i = 0$ ) caused by covalent chemical differences among the experimental samples.

The Ran-imp $\beta$  system in Fig. 6B provides an interesting counterpart to the A1-GPIb $\alpha$  complex discussed earlier. As in that example, the system is believed to exhibit two bound conformations with different adhesion strengths (35, 42). This is also supported by evidence of conformational variability in the crystal structure of a truncated imp $\beta$  bound to Ran-GppNHp, where two versions of the molecular complex were observed, characterized by substantially different sets of interactions (43). The bound conformations are expected to dynamically interconvert, but the timescale has not been measured. Our analysis of the existing data provides an upper bound on the rate,  $k_i < 6.4 \text{ s}^{-1}$ . We predict that further experiments could fix the rate more precisely: for example, by going to pulling velocities slower than  $v = 100 \text{ nm/s}$  (the slowest  $v$  in the current dataset), we may be able to observe PC, like in Fig. 2D, Middle, establishing the scale of  $k_i$ . This is opposite of the prescription we gave above for the A1-GPIb $\alpha$  complex, where the existing experiments have been too slow rather than too fast. Our theory thus provides a guide for experimentalists to fine-tune their

parameters to extract the most information possible from the system under study.

We envision that our approach will become one part of a larger, comprehensive experimental toolbox for investigating heterogeneity in biomolecules: it can test for and quantify heterogeneity based on the rupture force distributions, but these distributions do not contain all of the information we would like to know about a system. A large  $\Delta$  parameter indicates that there are multiple states in the intact/folded part of the free-energy landscape, and that these states must interconvert on timescales slower than the mean rupture time. To extract additional details, like the precise number of functional states, requires using other experimental/analytical techniques, like single-molecule FRET. One recent example where this was demonstrated was the  $k$ -means clustering algorithm applied by Hyeon et al. (16) to estimate the number of interconverting states from single-molecule FRET trajectories of a simple nucleic acid construct, the Holliday junction. In principle, this approach could be extended to folding trajectories obtained in constant force experiments, which in conjunction with the distribution of rupture forces could be used to extract the number of distinct functional states.

## Conclusions

Our work introduces a generic method for characterizing heterogeneity in biomolecules using rupture force distributions from force spectroscopy experiments. The central result is a single nondimensional parameter  $\Delta \geq 0$ . A system with no measurable

heterogeneity on the timescale of the pulling experiment has  $\Delta = 0$ . When  $\Delta > 0$ , its magnitude characterizes the degree of the disorder. Both in the presence and absence of heterogeneity, the method yields bounds on the local equilibration rate  $k_{\text{eq}}$  within a system state, and (if heterogeneity is present) the rate of interconversion  $k_i$  between states. The practical value of our approach is demonstrated by analyzing ten previous experiments, allowing us to classify a broad range of biomolecular systems. The five cases where heterogeneity was observed are all the more striking given the persistence of their conformational states, with upper bounds on  $k_i \lesssim 10 \text{ s}^{-1}$ .

Our theory leads to a proposal for future experimental studies: searching for a range of pulling speeds where the data exhibits the property of partial collapse, allowing for a more accurate determination of  $k_i$ . This PC scenario did not occur among the datasets we considered, although in two cases (the protein complexes A1-GPIb $\alpha$  and Ran-imp $\beta$ ) we predict that extending the

range of pulling velocities would very likely result in PC. The global energy landscapes of multidomain protein and nucleic acid systems are essential guides to their biological function, but are quite difficult to map out in the laboratory. This is particularly true for systems where the ruggedness of the landscape creates a host of long-lived, functional states. The approach described here suggests new ways in which single-molecule pulling experiments can be used to obtain information about internal dynamics of systems with functionally heterogeneous states. Our theory should shed light on both the static and dynamic aspects of such landscapes, the first step toward a comprehensive structural understanding of these biomolecular shape-shifters.

**ACKNOWLEDGMENTS.** This work was initiated when M.H. and D.T. were visiting scholars at Korea Institute for Advanced Study in 2013. We are grateful for the support from the National Science Foundation Award CHE 16-36424 (to D.T.).

- Altschuler SJ, Wu LF (2010) Cellular heterogeneity: Do differences make a difference? *Cell* 141(4):559–563.
- Lu HP, Xun L, Xie XS (1998) Single-molecule enzymatic dynamics. *Science* 282(5395):1877–1882.
- van Oijen AM, et al. (2003) Single-molecule kinetics of  $\lambda$  exonuclease reveal base dependence and dynamic disorder. *Science* 301(5637):1235–1238.
- English BP, et al. (2006) Ever-fluctuating single enzyme molecules: Michaelis-Menten equation revisited. *Nat Chem Biol* 2(2):87–94.
- Solomatin SV, Greenfield M, Chu S, Herschlag D (2010) Multiple native states reveal persistent ruggedness of an RNA folding landscape. *Nature* 463(7281):681–684.
- Kim J, Zhang CZ, Zhang X, Springer TA (2010) A mechanically stabilized receptor-ligand flex-bond important in the vasculature. *Nature* 466(7309):992–995.
- Buckley CD, et al. (2014) Cell adhesion. The minimal cadherin-catenin complex binds to actin filaments under force. *Science* 346(6209):1254211.
- Austin RH, Beeson KW, Eisenstein L, Frauenfelder H, Gunsalus IC (1975) Dynamics of ligand binding to myoglobin. *Biochemistry* 14(24):5355–5373.
- Frieden C (1979) Slow transitions and hysteretic behavior in enzymes. *Annu Rev Biochem* 48:471–489.
- Schmid FX, Blaschek H (1981) A native-like intermediate on the ribonuclease A folding pathway. 2. Comparison of its properties to native ribonuclease A. *Eur J Biochem* 114(1):111–117.
- Agmon N, Hopfield JJ (1983) Transient kinetics of chemical reactions with bounded diffusion perpendicular to the reaction coordinate: Intramolecular processes with slow conformational changes. *J Chem Phys* 78(11):6947–6959.
- Frauenfelder H, Parak F, Young RD (1988) Conformational substates in proteins. *Annu Rev Biophys Chem* 17(1):451–479.
- Honeycutt JD, Thirumalai D (1990) Metastability of the folded states of globular proteins. *Proc Natl Acad Sci USA* 87(9):3526–3529.
- Zwanzig R (1990) Rate processes with dynamical disorder. *Acc Chem Res* 23(5):148–152.
- Zwanzig R (1992) Dynamical disorder: Passage through a fluctuating bottleneck. *J Chem Phys* 97(5):3587–3589.
- Hyeon C, Lee J, Yoon J, Hohng S, Thirumalai D (2012) Hidden complexity in the isomerization dynamics of Holliday junctions. *Nat Chem* 4(11):907–914.
- Kowanko D, et al. (2015) Cation-induced kinetic heterogeneity of the intron-exon recognition in single group II introns. *Proc Natl Acad Sci USA* 112(11):3403–3408.
- Liu B, Baskin RJ, Kowalczykowski SC (2013) DNA unwinding heterogeneity by RecBCD results from static molecules able to equilibrate. *Nature* 500(7463):482–485.
- Pressé S, Lee J, Dill KA (2013) Extracting conformational memory from single-molecule kinetic data. *J Phys Chem B* 117(2):495–502.
- Raible M, Evstigneev M, Reimann P, Bartels FW, Ros R (2004) Theoretical analysis of dynamic force spectroscopy experiments on ligand-receptor complexes. *J Biotechnol* 112(1-2):13–23.
- Raible M, Reimann P (2006) Single-molecule force spectroscopy: Heterogeneity of chemical bonds. *EPL* 73(4):628–634.
- Raible M, et al. (2006) Theoretical analysis of single-molecule force spectroscopy experiments: Heterogeneity of chemical bonds. *Biophys J* 90(11):3851–3864.
- Hyeon C, Hinczewski M, Thirumalai D (2014) Evidence of disorder in biological molecules from single molecule pulling experiments. *Phys Rev Lett* 112(13):138101.
- Thirumalai D, Hyeon C (2005) RNA and protein folding: Common themes and variations. *Biochemistry* 44(13):4957–4970.
- Evans E, Ritchie K (1997) Dynamic strength of molecular adhesion bonds. *Biophys J* 72(4):1541–1555.
- Hu Z, Cheng L, Berne BJ (2010) First passage time distribution in stochastic processes with moving and static absorbing boundaries with application to biological rupture experiments. *J Chem Phys* 133(3):034105.
- Bullerjahn JT, Sturm S, Kroy K (2014) Theory of rapid force spectroscopy. *Nat Commun* 5:4463.
- Dudko OK, Hummer G, Szabo A (2006) Intrinsic rates and activation free energies from single-molecule pulling experiments. *Phys Rev Lett* 96(10):108101.
- Schlierf M, Rief M (2006) Single-molecule unfolding force distributions reveal a funnel-shaped energy landscape. *Biophys J* 90(4):L33–L35.
- Koch SJ, Wang MD (2003) Dynamic force spectroscopy of protein-DNA interactions by unzipping DNA. *Phys Rev Lett* 91(2):028103.
- Neuert G, Albrecht C, Pamir E, Gaub HE (2006) Dynamic force spectroscopy of the digoxigenin-antibody complex. *FEBS Lett* 580(2):505–509.
- Manosas M, Collin D, Ritort F (2006) Force-dependent fragility in RNA hairpins. *Phys Rev Lett* 96(21):218301.
- Bizarro CV, Alemany A, Ritort F (2012) Non-specific binding of Na<sup>+</sup> and Mg<sup>2+</sup> to RNA determined by force spectroscopy methods. *Nucleic Acids Res* 40(14):6922–6935.
- Wojcikiewicz EP, Abdulreda MH, Zhang X, Moy VT (2006) Force spectroscopy of LFA-1 and its ligands, ICAM-1 and ICAM-2. *Biomacromolecules* 7(11):3188–3195.
- Nevo R, Brumfeld V, Elbaum M, Hinterdorfer P, Reich Z (2004) Direct discrimination between models of protein activation by single-molecule force measurements. *Biophys J* 87(4):2630–2634.
- Strunz T, Oroszlan K, Schäfer R, Güntherodt HJ (1999) Dynamic force spectroscopy of single DNA molecules. *Proc Natl Acad Sci USA* 96(20):11277–11282.
- Bartels FW, Baumgarth B, Anselmetti D, Ros R, Becker A (2003) Specific binding of the regulatory protein ExpG to promoter regions of the galactoglucan biosynthesis gene cluster of *Sinorhizobium meliloti*—a combined molecular biology and force spectroscopy investigation. *J Struct Biol* 143(2):145–152.
- Fuhrmann A, Schoening JC, Anselmetti D, Staiger D, Ros R (2009) Quantitative analysis of single-molecule RNA-protein interaction. *Biophys J* 96(12):5030–5039.
- Alcaraz J, et al. (2002) Correction of microrheological measurements of soft samples with atomic force microscopy for the hydrodynamic drag on the cantilever. *Langmuir* 18(3):716–721.
- Janovjak H, Struckmeier J, Müller DJ (2005) Hydrodynamic effects in fast AFM single-molecule force measurements. *Eur Biophys J* 34(1):91–96.
- Liu R, Roman M, Yang G (2010) Correction of the viscous drag induced errors in macromolecular manipulation experiments using atomic force microscope. *Rev Sci Instrum* 81(6):063703.
- Nevo R, et al. (2003) A molecular switch between alternative conformational states in the complex of Ran and importin  $\beta$ 1. *Nat Struct Biol* 10(7):553–557.
- Vetter IR, Nowak C, Nishimoto T, Kuhlmann J, Wittinghofer A (1999) Structure of a Ran-binding domain complexed with Ran bound to a GTP analogue: Implications for nuclear transport. *Nature* 398(6722):39–46.
- Ermak DL, McCammon JA (1978) Brownian dynamics with hydrodynamic interactions. *J Chem Phys* 69(4):1352–1360.
- Van Kampen NG (2007) *Stochastic Processes in Physics and Chemistry* (Elsevier, Amsterdam).
- Neuman KC, Nagy A (2008) Single-molecule force spectroscopy: Optical tweezers, magnetic tweezers and atomic force microscopy. *Nat Methods* 5(6):491–505.
- Viani MB, et al. (1999) Small cantilevers for force spectroscopy of single molecules. *J Appl Phys* 86(4):2258–2262.